

How room-humidity during the coating affects the structural, optical and photocatalytic properties of TiO₂ films

M. E. de Anda Reyes · G. Torres Delgado ·
R. Castanedo Pérez · J. Márquez Marín ·
O. Zelaya Ángel

Received: 7 September 2011 / Accepted: 5 November 2011 / Published online: 16 November 2011
© Springer Science+Business Media, LLC 2011

Abstract TiO₂ thin films were obtained on glass slide substrates by the sol–gel technique. The substrates were coated by the immersion-removal method, at a constant withdrawal speed. The TiO₂ precursor solution and the substrate were maintained in a closed box with a controlled relative humidity (RH) during the removal of the substrate. The RH was varied in the 30–90% range in steps of 20%. The films were dried and after that sintered in an open atmosphere. The effect of the RH was studied on the structural, optical and photocatalytic properties. The films are polycrystalline with an anatase phase and show a high optical transmission in the UV–Vis range. The photocatalytic activity was evaluated by the photobleaching of methylene blue in an aqueous solution. The best photocatalytic activity was obtained for the films with 90% RH, this fact is mainly attributed to the highest porosity value obtained for these films.

Keywords TiO₂ · Photocatalysis · Room-humidity · Dipping · Sol–gel · Thin films

1 Introduction

TiO₂ is the wide band gap semiconductor more important for photocatalysis, which in turn, is applied to most processes for cleaning of polluted liquid and gaseous substances [1, 2]. The decontamination mechanism involves the generation of electron–hole carriers which migrate to the surface to activate redox reactions for the organic pollutants breakdown. Several procedures are carried out in order to enhance the efficiency of the photocatalytic activity of the materials, more utilized because of their better results are: (a) energy band gap coupling of two different materials to increase the charge carrier separation with the purpose to decrease the electron–hole recombination [3]. (b) The application of an external electric field to the photocatalytic oxide with the same aim of the previous case [4]. (c) The improvement of hydrophilic properties of surface of photocatalyst [5]. (d) By doping the material of the photocatalyst to diminish the band gap to use lower photo energy in the electron–hole pair generation [6] and (e) the increase of the effective area of contact between the photocatalyst and electrolyte, in this way the interchange of charge at the interface is increased [7]. With respect to the last mechanism different techniques have been employed to increase the contact effective area, among them can be cited: use of nanoneedles [7], preparing porous material [8], use of composites [9], etc. The advantages of or disadvantages of each technique are, after all, of economic aspect.

It is known that the stages involved during the sol–gel dip coating process have a strong influence on the structure of the deposited film [10, 11]. In particular, the overlap of the deposition and evaporation stages establishes a competition between evaporation (which compact the structure) and continuing condensation reaction. Since water is an

M. E. de Anda Reyes · G. Torres Delgado ·
R. Castanedo Pérez (✉) · J. Márquez Marín
Centro de Investigación y de Estudios Avanzados del I.P.N.,
Unidad Querétaro, A.P. 1-798, 76001 Querétaro, Qro., Mexico
e-mail: rcastanedo@qro.cinvestav.mx

O. Zelaya Ángel
Depto. de Física, Centro de Investigación y de Estudios
Avanzados del I.P.N., A.P. 14-740, 07360 México, D.F., Mexico

important parameter in the sol gel process, their presence at the time which the substrate is being removed from the precursor solution can modify the rates of the aggregation, gelation, and drying stages of the deposited film. Due to the ambient relative humidity (RH) changes depending on geographical location, is important to study the influence of this parameter on the physical properties of TiO₂ thin films when they are prepared by sol–gel technique. Influence of RH on the formation of TiO₂ films by dip-coating has been extensively studied in the case of mesoporous films [11]. Many protocols use controlled RH since then [12–14].

In this work a systematic study of the RH influence on the preparation of TiO₂ thin films by sol–gel technique is reported. The humidity effect on the preparation of TiO₂ films is observed in the physical properties of the material which in turn have strong influences on its photocatalytic activity (PA), here PA is determined by means of the bleaching of methylene blue (MB) aqueous solutions. We have observed that the larger the ambient humidity, the larger the PA of TiO₂. The increasing of PA in our samples can be associated with the increase of porosity in the oxide, as porosity increases when RH increases. The decreasing of rate evaporation when RH increases during the film deposition left liquid solution in the volume of the layers, in such a way that when annealing is carried out, liquid phases evaporate leaving it porous into the volume of material [11, 15]. RH is varied in the range 30–90% in 20%-steps and the better PA is observed when RH reached 90%. Therefore, by increasing the RH, hence, the contact effective surface of photocatalyst, during the growth process PA is increased.

2 Experimental details

The precursor solution used to obtain TiO₂ thin films was prepared starting from the following reagents: for each mol of titanium isopropoxide (TIP), 36.46 mol of ethanol, 0.4696 mol of nitric acid and 3 mol of deionized water were used. Two solutions were prepared separately; one was formed by mixing half of the ethanol with both water and acid at room temperature (RT). This solution and the remaining ethanol were introduced into a gloves-box. The ethanol was mixed with the TIP by using magnetic stirring in a N₂ atmosphere. Finally, both solutions were mixed while maintaining the stirring. The resulting solution was transparent with a light yellowish color and the gelation time was longer than 7 days. The RH during the coating procedure was controlled by a device designed in our laboratory (Fig. 1). This device is constituted of an acrylic box, a cooling system (for the Peltier cell) and a controller process. Inside of the box, there are a humidifier and a humidity sensor.

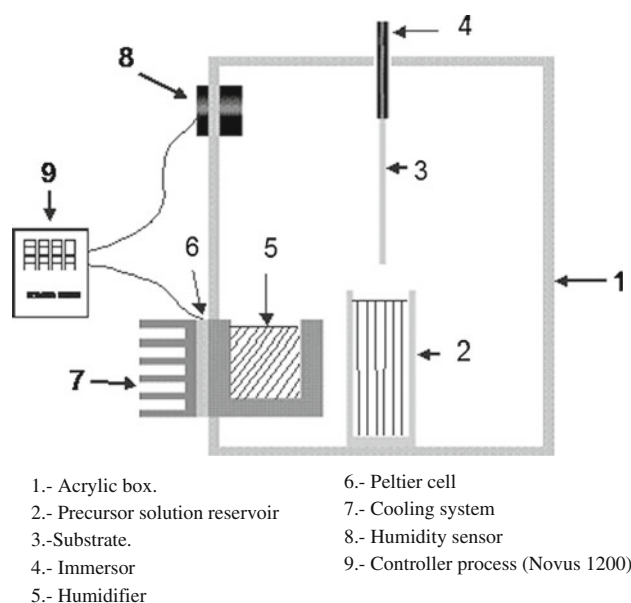


Fig. 1 Scheme of the humidity controller device

The films were deposited using the immersion-removal method. The removal speed was 6 cm/min. The relative humidity was varied in the 30–90% range in steps of 20%. The precursor solution was put inside of the humidifier device and the glass slide substrate was collocated into the device through a small entrance of the box (superior part of the device, part 4 in Fig. 1). The substrate was put into the precursor solution and removal at constant velocity. The films were obtained from five coatings, after each coating the samples were dried at 250 °C for 2 min. The substrate or substrate + coating remained in the selected humidity before each thermal treatment at 250 °C for 3.5 min. The five coatings were successive. After that, the films were preheated in a muffle furnace at 100 °C for 60 min and subsequently sinterized at 500 °C. The films were kept inside the furnace during the sintering treatment until the RT was reached.

The X-ray diffraction (XRD) studies were carried out in a Rigaku D/max-2100 (CoK_{α1} radiation 1.78899 Å) with a thin film attachment. The UV–Vis spectra of the films were measured on a Perkin-Elmer Lambda-2 spectrometer in the 300–1,100 nm wavelength range. It was used a glass as reference. The IR spectra of the films were measured on a Perkin Elmer Spectrum GT FTIR system, using a device of attenuated total reflection in the middle IR range. The PA was evaluated by the photobleaching of MB in an aqueous solution. 3 mL of a MB solution at initial concentration of 2.5×10^{-5} mol/L was put in a $1 \times 1 \times 4$ cm³ quartz cell. A rectangular sample (area = 1.8 cm²) was immersed into the cell and this arrangement, the cell + solution + sample was exposed to UV light. A G15T8 germicidal lamp with power of 15 W was used, as the UV excitation source. The

distance between cell and lamp was 4.0 cm and the irradiation times (t_i) were 1, 2, 3, 4 and 5 h. In order to quantify the PA, optical absorption spectra of the residual MB were measured for the different irradiation times in the range of 418–750 nm, using an Agilent spectrometer/8454 model. The residual MB concentration ([MB]) was determined following Beer-Lambert's law for absorption band with the maximum at 660 nm. Integrated area under each spectrum was used to determine the PA (the quantity of MB degradation) of each sample: lower [MB], higher MB degradation, hence, higher PA. The [MB] was normalized with respect to the [MB] at irradiation time, $t = 0$ ([MB]₀).

3 Results and discussion

XRD patterns of the films as a function of RH are shown in Fig. 2. The films are polycrystalline and the diffraction peaks look like to the powder pattern of the TiO₂ anatase phase. A preferential orientation is not observed for all the films. The relative intensity of the diffraction peaks does not change with the RH, however, there is a little increase of the full-width at half-maximum (FWHM), as the RH increases. Using Scherrer's formula and the FWHM of the three main diffraction peaks, corresponding to (101), (004) and (200) crystalline planes, the average grain size (GS) is

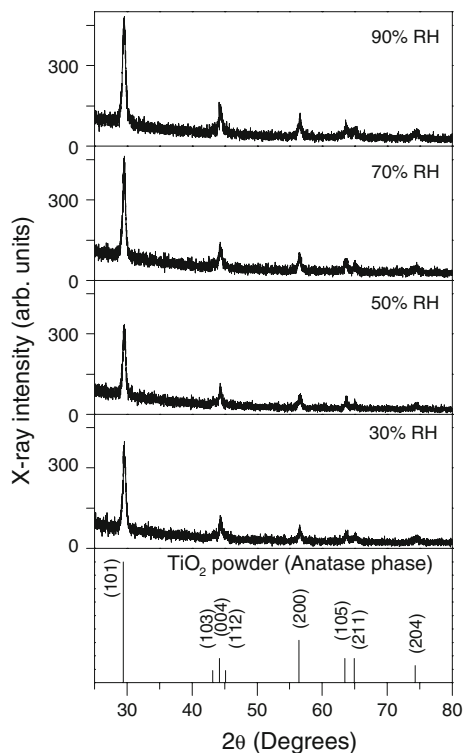


Fig. 2 XRD patterns of the TiO₂ films for all the humidity percentages studied

Table 1 Grain size and, direct and indirect band gap energy values of the TiO₂ films for the humidity percentages studied

RH (%)	GS (nm)	Direct gap (eV)	Indirect gap (eV)
30	27.7	3.64	3.49
50	26	3.63	3.49
70	23.4	3.65	3.52
90	20.8	3.59	3.44

calculated. The GS decreases from an average value of 28–21 nm as the RH increases (Table 1). Optical transmission spectra of the films at the different RH studied are shown in Fig. 3. All the films show a high transparency around 70%. As well, a direct and indirect band gap are calculated by employing the optical absorption coefficient (α) as a function of the photon energy ($h\nu$) obtained from the absorption spectra of the films and the relationships $(\alpha h\nu)^2 = A(E_g - h\nu)$ and $(\alpha h\nu)^{1/2} = A(E_g - h\nu)$. The direct band gap energy is practically constant around 3.64 eV except for the lower value of 3.59 eV which is obtained for the films with the highest RH value (Table 1). These values are inside of the range reported by Hasan et al. [16].

The oscillations observed in the spectra are due to interference effects, which is evidence of the high uniformity of the films thickness. The increase of these oscillations with the RH is an indication of an increase of the

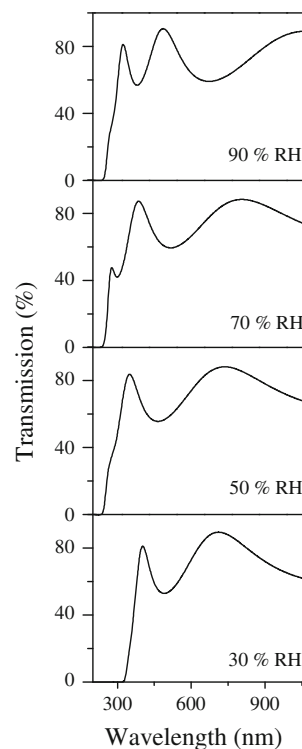


Fig. 3 Optical transmission spectra of the TiO₂ films for all the humidity percentages studied

film’s thickness. The thickness (τ) of the films is determined by means of optical transmission spectra starting from the maxima and minima of interference and using the following equation [17]

$$\tau = \frac{i(\lambda_0\lambda_1)}{2n(\lambda_0 - \lambda_1)} \tag{1}$$

where i is the number of minima (maxima) between maxima (minima) located between λ_0 and λ_1 wavelengths, and n is the refractive index which is calculated using the average transmission values obtained from the transmission spectra [18]. The n and τ values as a function of the RH are shown in Fig. 4. Higher thicknesses are obtained as the RH increases in accordance with data observed from the transmission spectra. On the other hand, the n value decreases as the RH increases from 2.2 to 2.0, these values are lower than the one of 2.52 reported for monocrystalline TiO₂, free of pore [19] and with an n reported value of 2.3 for TiO₂ films deposited by sputtering [16]. The decrease of n is related with an increase of the porosity of the films. The porosity was calculated using the following equation [20]:

$$\text{Porosity}(\%) = \left(1 - \frac{n^2 - 1}{n_d^2 - 1}\right) \times 100 \tag{2}$$

where n_d is the refractive index of pore-free anatase [19], and n is the refractive index of our porous thin films.

The values of porosity are shown in Fig. 5. The porosity increases from 29 to 41% for the humidity range of 30–90% studied.

The [MB] normalized as a function of the t_i for the different values of RH is shown in Fig. 6. As can be seen,

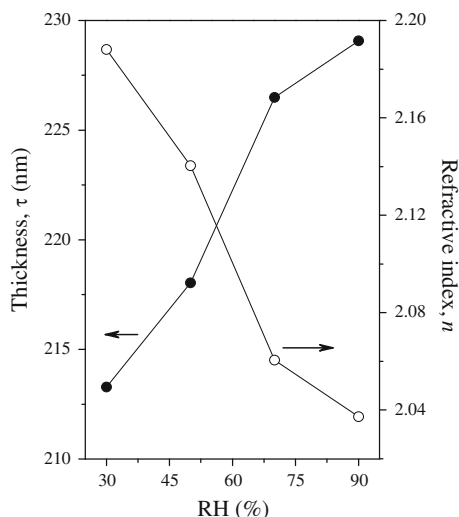


Fig. 4 Behavior of refractive index (n) and the thickness (τ) as a function of the relative humidity (RH)

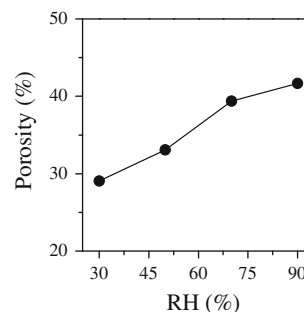


Fig. 5 Porosity values as a function of the RH

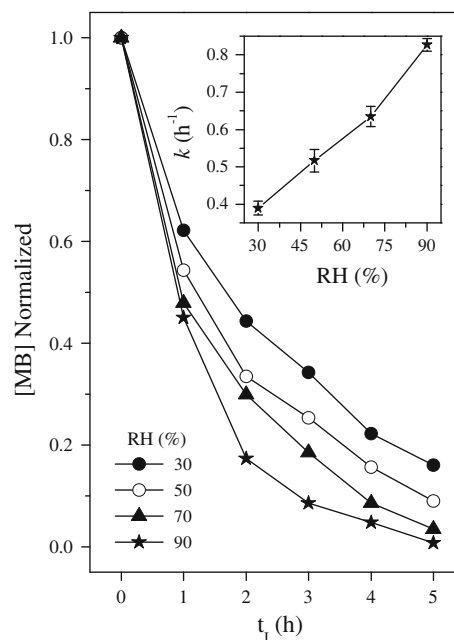


Fig. 6 Methylene blue concentration [MB] as a function of the irradiation time for all the humidity percentages studied. The [MB] has been normalized. The inset shows the dependence of rate constant k as a function of the RH

[MB] normalized vs t_i as an exponential decay, characteristic of a first order reaction:

$$[\text{MB}] = [\text{MB}]_0 e^{-kt_i} \tag{3}$$

where k is the rate constant, $[\text{MB}]_0$ is the initial MB concentration ($=1$), and t_i is the irradiation time. By means of a fitting to exponential decay, the rate constant is evaluated for all the samples. In the inset of Fig. 6, it is shown the k (h^{-1}) values as a function of the RH. As can be seen from this figure, the PA of the films is considerably increased as the RH increases. This increase of the PA can be associated to the increase of porosity of the films as the RH increases. The little decrease of the crystalline grain does not provoke detriment on the PA due to the parameter for highest change is the porosity.

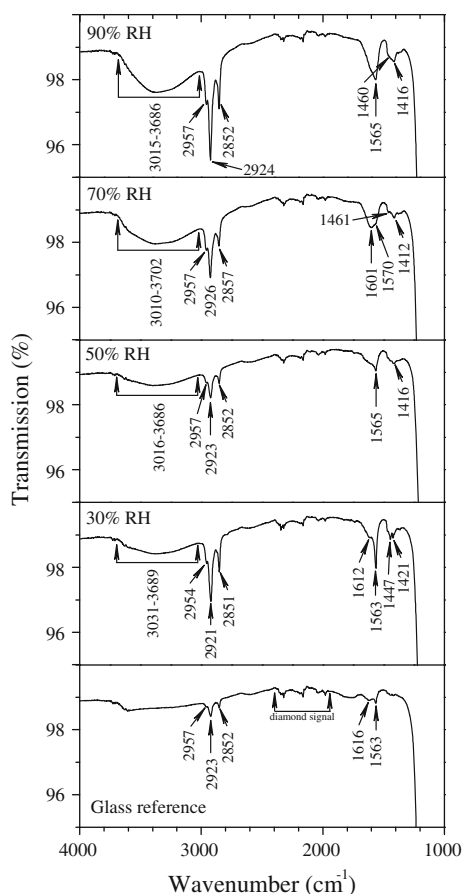


Fig. 7 FTIR spectra of the films for all the humidity percentages studied

Table 2 The vibrational modes observed in the IR spectra and their wavenumber corresponding

Wavenumber (cm ⁻¹)	Vibrational modes
3,387 and 3,236 [16]	–OH stretching
1,628 [16]	Adsorbed H ₂ O molecules
2,915 [17]	CH ₂ groups
1,650–1,280 [18]	Induced by residue organic groups
2,800 [19, 20]	Bending of water

Fourier transform infrared (FTIR) spectra of all the samples studied are displayed in Fig. 7, this measurement is carried out after the annealing at 500 °C in air. Different vibrational signals are labeled in the spectra which correspond to modes of several species present in the volume of the material. In Table 2 are compiled the data and are classified as reported in the literature [21–25]. It is important to notice that the broad band in the interval 1,515–3,700 cm⁻¹, which has been associated to O–H bonds coming from the dissociative adsorption of H₂O in TiO₂ [26], in our spectra, this band increases the intensity as RH increases. This result supports the fact that RH

reduces the evaporation during the removing of substrate plus film from the growing solution. As aforementioned, the volume occupied by that residual-solution becomes void after sintering at 500 °C in air. In this manner, the material increases the porosity.

In all the process, phenomena occur as follow: GS decreases when RH increases since O–H's population increases also, and as OH's tend to situate on the surface of GS causes a decreasing of the rate of GS-growth [11, 27]. Porosity increases when RH rises because larger volume of vapor is trapped into the film, which evaporates with annealing, leaving a more porous material [11]. Larger porosity means larger effective surface in contact with electrolyte, then PA increases.

4 Conclusions

The structural and optical properties of the TiO₂ don't show important changes with the RH during the coating of the films. However, the thickness, porosity and PA of the films significantly increase with this parameter. The photodegradation of MB follows a first order reaction. The rate constant shows an important change from 0.38 to 0.82 as the RH increases. The films with highest PA correspond to the films deposited with an RH of 90%, i.e. films with highest porosity.

Acknowledgments This work was supported by Consejo Nacional de Ciencia y Tecnología (CONACYT) under Project CB-2008-106912 and Instituto de Ciencia y Tecnología del Distrito Federal (ICYTDF) under Project PICCO10-81. The authors also thank CONACYT for the fellowship awarded to M. Sci. M. E. de Anda Reyes. The authors wish to thank to M. Sci. C. I. Zúñiga Romero for her technical assistance.

References

1. Hashimoto K, Irie H, Fujishima A (2005) TiO₂ photocatalysis: a historical overview and future prospects. *Jpn J Appl Phys* 44:8269–8285
2. Linsebigler AL, Lu G, Yates JT Jr (1995) Photocatalysis on Ti on surfaces: principles, mechanisms, and selected results. *Chem Rev* 95:735–758
3. Mayén-Hernández SA, Torres-Delgado G, Castanedo-Pérez R, Mendoza-Alvarez JG, Zelaya-Angel O (2007) Effect of the sintering temperature on the photocatalytic activity of CdO + Cd-TiO₃ thin films. *J Adv Oxid Technol* 10:85–89
4. Zhang W, An T, Cui M, Sheng G, Fu J (2005) Effects of anions on the photocatalytic and photoelectrocatalytic degradation of reactive dye in a packed-bed reactor. *J Chem Technol Biotechnol* 80:223–229
5. Li X, Xiong R, Wei G (2008) S–N Co-doped TiO₂ photocatalysts with visible-light activity prepared by sol–gel method. *Catal Lett* 125:104–109
6. Luu CL, Nguyen QT, Ho ST (2010) Synthesis and characterization of Fe-doped TiO₂ photocatalyst by the sol–gel method. *Adv Nat Sci Nanosci Nanotechnol* 1:015008

7. Yang JL, SJ An, Park WI, GY Yi, Choi W (2004) Photocatalysis using ZnO thin films and nanoneedles grown by metal-organic chemical vapor deposition. *Adv Mater* 16:1661–1664
8. Wongcharee K, Brungs M, Chaplin R, Hong YJ, Sizgek E (2004) Influence of surfactant and humidity on sol–gel macroporous organosilicate coatings. *J Sol Gel Sci Technol* 29:115–124
9. Negishi N, Takeuchi K, Ibusuki T (1998) Surface structure of the TiO₂ thin film photocatalyst. *J Mater Sci* 33:5789–5794
10. Brinker CJ (1990) Sol–gel science: the physics and chemistry of sol–gel processing. Academic Press, London, p 797
11. Crepaldi EL, Soler-Illia GJAA, Grosso D, Cagnol F, Ribot F, Sanchez C (2003) Controlled formation of highly organized mesoporous titania thin films: from mesostructured hybrids to mesoporous nanoanatase TiO₂. *J Am Chem Soc* 125:9770–9786
12. Samie L, Beitollahi A, Faal-Nazari N, Akbar Nejad MM, Vinu A (2011) Effect of humidity treatment on the structure and photocatalytic properties of titania mesoporous powder. *J Mater Sci Mater Electron* 22:273–280
13. Chang YS, Lee Y-C, Yuhara Junji, Chan LH, Teoh LG, Chen HM (2011) Effect of water on the formation of nanostructured mesoporous titania. *Curr Appl Phys* 11:486–491
14. Neyshtadt S, Frey GL (2011) Synthesis of ordered mesostructured TiOx thin films from tetrahydrofuran–water solutions. *Microporous Mesoporous Mater* 142:708–715
15. Fernandez-Martin C, Edler KJ, Roser SJ (2004) Humidity and temperature effects on CTAB-templated mesophase silicate films at the air–liquid interface. *Langmuir* 20:10679–10684
16. Hasan MM, Haseeb ASMA, Saidur R, Masjuki HH, Hamdi M (2010) Influence of substrate and annealing temperatures on optical properties of RF-sputtered TiO₂ thin films. *Opt Mater* 32:690–695
17. Runyam WR (1975) Semiconductor measurements and instrumentation. Mc Graw Hill, Nueva York, p 166
18. Pankove JI (1971) Optical processes in semiconductors. Dover Publications Inc, New York, pp 94–95
19. Kingery WD, Bowen HK, Uhlmann DR (1976) Introduction to ceramics, 2nd edn. Wiley, New York, p 669
20. Yoldas BE, Partlow PW (1985) Formation of broad-band anti-reflective coatings on fused silica for high-power laser applications. *Thin Solid Films* 129:1–14
21. Ivanda M, Music S, Popovic S, Gotic M (1999) XRD, Raman and FTIR spectroscopic observations of nanosized TiO₂ synthesized by the sol–gel method based on an esterification reaction. *J Mole Struct* 480–481:645–649
22. Jin M, Zhang X, Emeline AV, Numata T, Murakami T, Fujishima A (2008) Surface modification of natural rubber by TiO₂ film. *Surf Coat Technol* 202:1364–1370
23. Zhang W-J, He Y-Q, Qi Q (2005) Synthesize of porous TiO₂ thin film of photocatalyst by charged microemulsion templating. *Mater Chem Phys* 93:508–515
24. Janitabar-Darzi S, Mahjoub AR (2009) Investigation of structural, optical, and photocatalytic properties of mesoporous TiO₂ thin films synthesized by sol gel templating technique. *Physica E* 42:176–181
25. Schrijnemakers K, Impens NREN, Vansant EF (1999) Deposition of a titania coating on silica by means of the chemical surface coating. *Langmuir* 15:5807–5813
26. Bezrodna T, Puchkovska G, Shymanovska V, Baran J, Ratajzak H (2004) IR-analysis of H-bonded H₂O on the pure TiO₂ surface. *J Mole Struct* 700:175–181
27. Bagheri Garmarudi A, Khanmohammadi M, Khoddami N, Shabani K (2010) Feasibility investigation of near infrared spectrometry for particle size estimation of nano structures. *World Acad Sci Eng Technol* 70:636–638